Chemistry–A European Journal
Research Article
doi.org/10.1002/chem.202302970
Chemistry Europe
European Chemical Societies Publishing
www.chemeurj.org

Phosphonium-substituted Diphosphaindenylide (PPI): Exploration of Biradical Character and Ligand Properties

Peter Coburger,*[a] David Zuber,[a] Clara Schweinzer,[b] and Moritz Scharnhölz[b]

Dedicated to Evamarie Hey-Hawkins and Hansjörg Grützmacher on the occasion of their retirement.

Starting from $C_6H_4(PCl_2)_2$ and the TMS-substituted ylide $(TMS)_2C{=}PR_3$ (TMS = trimethylsilyl, R = *p*-tolyl), the phosphonium-substituted diphosphaindenylide **PPI** was prepared in two steps. CASSCF calculations as well as the reactivity toward diphenyl acetylene suggest a notable biradical character in **PPI**. Reaction with $[Cr(CO)_3(MeCN)_3]$ affords the complex $[Cr(CO)_3(\eta^5\text{-}\mathbf{PPI})]$ (**5**). This complex was employed to explore the ligand properties of **PPI**, which demonstrates considerable potential through the combination of strong metal-ligand interactions and the possibility of a pronounced indenyl effect.

Introduction

The indenyl anion, $[C_9H_7]^-$, is a frequently encountered η^5-coordinating ligand in transition metal chemistry. It can be viewed as a benzannulated derivative of the commonly known cyclopentadienide anion, $[C_5H_5]^-$. However, in contrast to $[C_5H_5]^-$, complexes of $[C_9H_7]^-$ exhibit more facile $\eta^5{-}\eta^3$ hapticity changes through a ring-slip mechanism (Figure 1). This phenomenon is called the "indenyl effect".[1,2] This effect leads to accelerated exchange reactions at the coordinated metal center via an associative mechanism, often resulting in enhanced catalytic activity compared to cyclopentadienide complexes.[3,4]

In recent years, there has been a renewed interest in studying the coordination chemistry of electron-poor ylidic derivatives of $[C_5H_5]^-$.[5–8] In these derivatives, one or more H-atoms are replaced with cationic moieties, such as sulfonium, imidazolium or phosphonium groups. It has been found that already the addition of neutral electron-withdrawing groups to $[C_5H_5]^-$ renders the resulting metal complexes rather electron-deficient. This electron deficiency has proven advantageous for catalytic transformations of electron-rich substrates.[9–11] Therefore, the utilization of even more electron-deficient, zwitterionic indenylide ligands holds great potential for further enhancing the activation of electron-rich substrates, by combining the indenyl effect with electron-poor, Lewis-acidic metal centers.

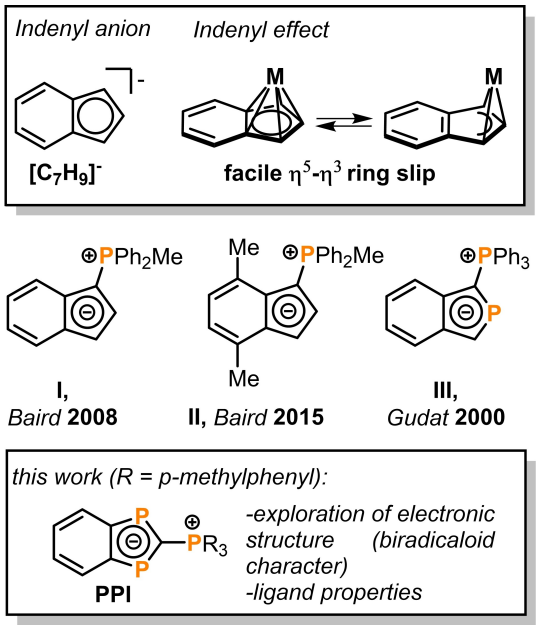

Figure 1. Top: Indenyl anion and schematic representation of the indenyl effect; middle: examples of phosphonium-substituted indenyl derivatives; bottom: PPI ligand reported in this work.

Baird and colleagues have reported two archetypal examples of phosphonium-indenylides (**PHIN**), **I** and **II**, and demonstrated their coordination properties toward Cr, Ru, and Ir.[12–14] Nevertheless, it is important to note that the electron-poor nature of these indenylide ligands may have a drawback. In a recent review, Kunz highlighted that complexes of zwitterionic cyclopentadienylides and indenylides form weaker metal-arene bonds then the original $[C_5H_5]^-$ and $[C_9H_7]^-$ anions.[6] This limitation might curtail their widespread application in reactivity studies and catalysis.

We therefore reasoned that the isolobal replacement of endocyclic CH groups by P atoms in zwitterionic indenylides might strengthen the metal-arene interaction by increasing the π-acceptor properties of the resulting phosphaindenylide

[a] Dr. P. Coburger, D. Zuber
Department of Inorganic Chemistry, TU München, Lichtenbergstraße 4, 85747 Garching (Germany)
E-mail: peter.coburger@tum.de
[b] C. Schweinzer, Dr. M. Scharnhölz
Department of Chemistry and Applied Biosciences, ETH Zürich
Vladimir-Prelog-Weg 1, 8093 Zürich (Switzerland)

Supporting information for this article is available on the WWW under https://doi.org/10.1002/chem.202302970

ligand. Introduction of one phosphorus atom was studied previously by Gudat and colleagues who reported a phosphonium-substituted phosphaindenylide species and its coordination chemistry toward group 6 and 7 carbonyls (**III**, Figure 1).[15–17] In this study, we aim to build upon these findings by introducing a second endocyclic P-atom, resulting in the zwitterionic diphosphorus-substituted indenyl ligand **PPI**. Our combined experimental and theoretical investigation reveals that the addition of the second endocyclic P-atom leads to an interesting electronic structure which warrants **PPI** to be described as a P-centered biradicaloid. Furthermore, the ligand properties of **PPI** are evaluated based on a η^5-coordinated chromium tricarbonyl complex, [Cr(CO)$_3$(η^5-**PPI**)]. As such, **5** is a rare complex incorporating a π-bonded biradicaloid.[18–20] In this complex, **PPI** demonstrates strong binding as both a π-donor and a π-acceptor ligand. Notably, the benzannelation of the five-membered C_3P_2 ring significantly influences the structure of [Cr(CO)$_3$(η^5-**PPI**)], suggesting the potential for a pronounced indenyl effect in this complex.

Results and Discussion

Starting from 1,2-bis(dichlorophosphaneyl)benzene (**1**), **PPI** was synthesized following a two-step procedure (Scheme 1). First, treatment of **1** with the TMS-substituted ylide **2** in 1,2-difluorobenzene, DFB, affords the bis(chlorophosphane) **3**. Such TMS-substituted ylides have recently been used by the Grützmacher group and their further utilization for the preparation of P-heterocycles will be reported soon.[21] The bis(chlorophosphane) **3** was isolated in 91% yield as the diasteriomerically pure *meso* isomer (*vide infra*). In the $^{31}P\{^1H\}$ NMR spectrum of **3** in THF-d_8, the endocyclic PCl moieties give rise to a doublet at 133.9 ppm, while the P(*p*-tol)$_3$ group appears as a triplet at 26.2 ppm ($^2J_{PP}$ = 120 Hz). Finally, reduction of **3** with a slight excess of magnesium in THF results in the formation of **PPI**. Subsequently, this species was isolated as a yellow solid with the composition **PPI**·(MgCl$_2$)$_{0.3}$ in 39% yield. Compared to **3**, the endocyclic P atoms in **PPI** experience a considerable downfield shift of Δδ = 78.7 ppm (δ = 212.7 ppm) in the $^{31}P\{^1H\}$ NMR spectrum while the resonance of the P(*p*-tol)$_3$ group is only shifted moderately (δ = 24.7 ppm, Δδ = −1.5 ppm, $^2J_{PP}$ = 88 Hz). The shift of the endocyclic P atoms falls in the typical region expected for π-conjugated P heterocycles.[22] In the $^{13}C\{^1H\}$ NMR spectrum, the two quaternary carbon atoms of the central six-membered ring appear as a multiplet at 172.0 ppm and the triphosphorus-substituted quaternary carbon atom of the C_3P_2 ring shows a shift of 145.0 ppm (q, $^1J_{CP}$ = 71 Hz).

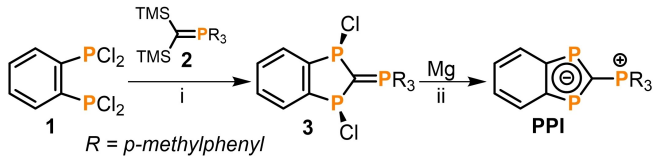

Scheme 1. Synthesis of **PPI**. Conditions: i, DFB, 16 h, r.t.; ii, THF, 24 h, r.t.

After recrystallization from THF/hexane, single crystals of **3** and **PPI** suitable for X-ray diffraction measurements were obtained.[23] The resulting solid-state structures are shown in Figure 2 together with selected distances and angles. As expected, the P–C bonds connecting the benzene moiety with the P_2Cl_2C–PR_3 fragment fall within the range of a typical single bond (P1–C3: 1.825(3) Å, P2–C2: 1.813(4) Å).[24] The triphosphorus-substituted carbon atom of the C_3P_2 ring, C1, exhibits a minor deviation from an ideal trigonal-planar environment (sum of bond angles: 358.7°) and shows an exocyclic P–C distance of 1.725(3) Å, suggesting some P=C double bond character. Furthermore, the endocyclic P–C1 distances are rather short, while the P–Cl bonds are elongated compared to standard single bonds ($\emptyset_{P-C1}$: 1.76 Å, $\emptyset_{P-Cl}$: 2.168 Å).[24] These observations might be explained by negative hyperconjugation from C1 into antibonding P–Cl σ* orbitals.[25] Reduction of **3** to **PPI** causes a significant shortening of the P1–C3 and P2–C2 distances to 1.763(2) Å and 1.768(2) Å, respectively. Now, the C–C as well as all P–C distances within the five-membered C_3P_2 ring are between the values expected for isolated single and double bonds (C2–C2: 1.429(3) Å, $\emptyset_{P-C}$: 1.76 Å)[24] and are thus indicative of π-conjugation. Furthermore, C1 again exhibits a trigonal-planar environment (sum of bond angles: 359.6°), and the exocyclic P–C distance is approximately 0.03 Å longer compared to **3**. Altogether, the comparison of the X-ray diffraction data of **3** and **PPI** indicates the presence of a π-conjugated, anionic $C_7H_4P_2$ core and an exocyclic cationic phosphonium moiety in **PPI**.

This zwitterionic description is further corroborated by DFT and TDDFT calculations, using the ORCA program package,[26] in combination with UV-vis spectroscopy (see the SI, section 4.2).

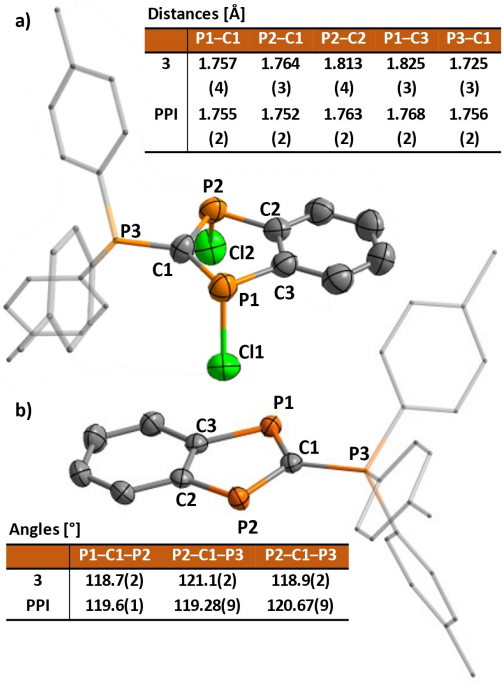

Figure 2. Solid-state structures of **3** (a) and PPI (b) together with selected distances and angles. Ellipsoids are at the 65% probability level. Hydrogen atoms are omitted and P(*p*-tol)$_3$ groups are drawn as transparent wireframes.

In particular, the UV-vis spectrum is dominated by charge-transfer (CT) transitions from the anionic $C_7H_4P_2$ core to the cationic phosphonium moiety (see the SI, section 4.4).

In addition to the zwitterionic character, our calculations also reveal the aromaticity of **PPI** based on magnetic and electron delocalization descriptors. The NICS(0) values of the central C_6 and C_3P_2 rings are −7.6 and −8.1, respectively, and the FLU-π index, a measure of π-electron delocalization, was calculated to 0.051(C_6) and 0.006 (C_3P_2). All these values fall within the range commonly found for aromatic hydrocarbons.[27,28]

So far, all experimental and theoretical data point toward a rather simple bonding description in **PPI**; namely an aromatic bicyclic $C_7H_4P_2$ core comprised of ten delocalized π-electrons bearing an exocyclic phosphonium moiety. Formally, the central six-membered C_6 ring contributes six π-electrons, while the annulated P_2C moiety contributes four π-electrons to the π-system in **PPI**. However, CASSCF calculations reveal a more intricate bonding situation in **PPI**. Specifically, the active space of the CASSCF calculation was chosen to comprise the 4π electrons of the annulated P_2C fragment in three orbitals [CAS(4,3)]. When these orbitals are expressed as localized orbitals, the direct contribution of individual Lewis-structures to the overall wavefunction of **PPI** can be evaluated (Scheme 2, see the SI, section 4.3). These calculations show that a biradical structure, **PPI-A**, has the highest individual weight of 42%, followed by the degenerate "covalent" structures **PPI-B** and **PPI-B'** (43% in total). **PPI-A** involves two radical centers, located at each endocyclic P atom, which exhibit antiferromagnetic coupling. The remaining Lewis-structures **PPI-C**, **PPI-C'** and **PPI-D** involve a considerable amount of charge separation and thus only exhibit minor contributions to the overall wavefunction (14% in total). For disulfur dinitride, N_2S_2, a textbook example of a p-block biradicaloid,[29,30] the total contributions of biradicaloid Lewis-structures amount to 46–48% using a similar CASSCF approach.[31,32]

When the CAS(4,3) calculation is carried out with natural orbitals, another commonly used measure of biradical character, the β-index, is obtained [see the SI, section 4.2 for results using CAS(2,2) and CAS(10,9)].[33] Here, a value of 12% is found. Again, a similar value was calculated for the heterocycle N_2S_2 (14%).[32] However, larger values were found for five-membered 2-aza-1,3-diphosphaindane-1,3-diyls (18%)[34] which are structurally related to **PPI**, and the four-membered biradicaloid [P(μ-NTer)]$_2$ (28%).[35,34] Based on these comparisons, **PPI** can be described as a P-centered biradicaloid with modest biradical character comparable to N_2S_2.

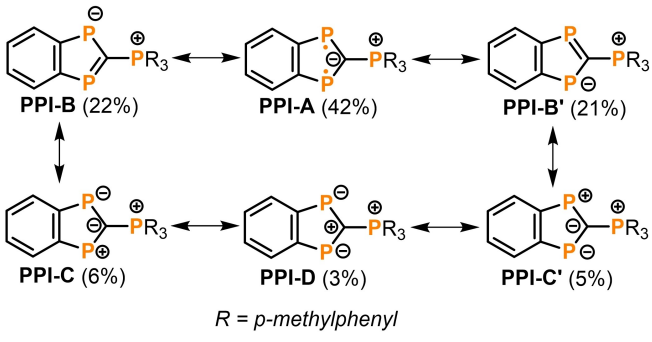

Scheme 2. Contributions of individual Lewis-structures based on a CAS(4,3) calculation using localized orbitals.

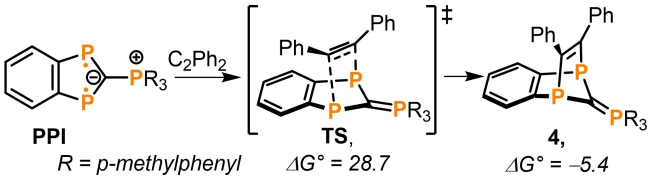

Scheme 3. Reactivity of **PPI** toward diphenyl acetylene. Calculated Gibbs free energies (electronic energies: M06-2X-D3(0)/def2-TZVP, CPCM(THF), thermal corrections: BP86-D3BJ/def2-SVP) are given in kcal mol^{-1} and **PPI** + C_2Ph_2 was used as the reference.

Experimentally, the biradical character of **PPI** can be probed by the reaction of diphenyl acetylene which yields the cycloaddition product **4** (Scheme 3). These addition reactions are characteristic of P-centered biradicaloids.[36–38] Although a solid-state structure of **4** was not obtained, we were able to characterize it accurately using mass spectrometry and NMR spectroscopy (see the SI, section 1). Notably, the addition of diphenyl acetylene causes a remarkable upfield shift of the endocyclic P atoms and the triphosphorus-substituted carbon atom of the C_3P_2 ring ($\Delta\delta(^{31}P) = -148.7$ ppm, $\delta(^{31}P) = 63.9$ ppm, $^2J_{PP} = 102$ Hz; $\Delta\delta(^{31}C) = -97.5$ ppm, $\delta(^{13}C) = 47.5$ ppm, $^1J_{PP} = 110$, 25 Hz). These upfield shifts are in line with the shifts predicted by DFT (see the SI, section 4.4). Additionally, the former triple bonded carbon atoms in C_2Ph_2 experience a downfield shift of 77.9 ppm and appear as a multiplet at $\delta(^{13}C) = 166.9$ ppm. For the biradicaloid [P(μ-NTer)]$_2$, the addition of acetylenes occurs spontaneously at room temperature.[36] However, in line with its lower biradical character, the reaction of C_2Ph_2 with **PPI** requires heating to 55 °C for 60 hours to achieve complete conversion. Our DFT calculations support this observation and predict an activation barrier ($\Delta G^{\ddagger}$) of 28.7 kcal mol^{-1} for the concerted cycloaddition (Scheme 4).

Having explored the electronic structure of **PPI**, we turned to investigate its ligand properties. For the indenyl anion $[C_9H_7]^-$ and its zwitterionic derivatives **I** and **III**, η^5-coordinated $Cr(CO)_3$ complexes are known (**I**: C_9H_6–PPh_2Me, **III**: $C_8H_5P_1$–PPh_3).[12,15,39] Therefore, an attempt was made to prepare a similar chromium tricarbonyl complex to compare and classify the ligand properties of **PPI**.

Gratifyingly, treatment of **PPI** with $[Cr(CO)_3(MeCN)_3]$ afforded the anticipated complex $[Cr(CO)_3\{\eta^5$-**PPI**$\}]$ (**5**, Scheme 4), which

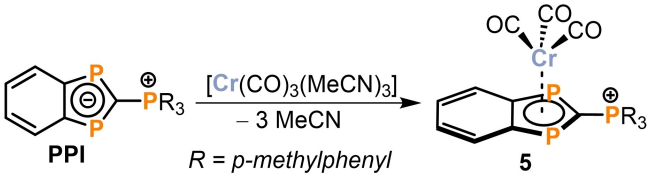

Scheme 4. Preparation of chromium tricarbonyl complex **5**.

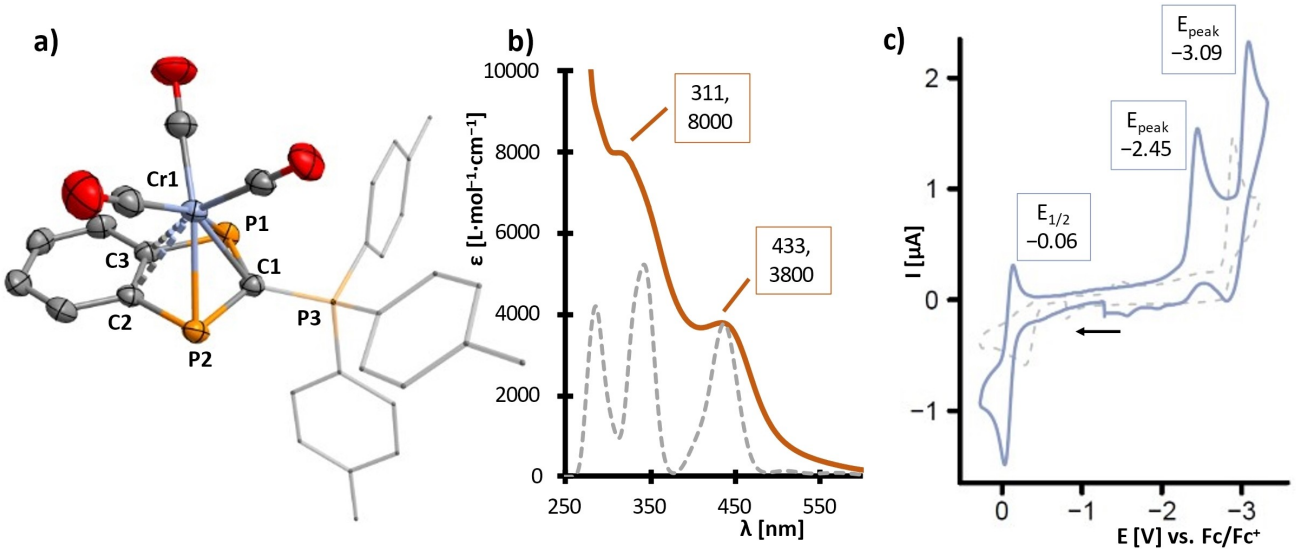

Figure 3. Selected analytical and calculated data for **5**. a) Molecular structure with ellipsoids at the 65 % probability level. Hydrogen atoms are omitted and P(*p*-tol)$_3$ groups are drawn as transparent wireframes. Selected distances [Å] and angles [°]: Cr1–P1 2.4149(8), Cr1–C1 2.168(2), Cr1–P2 2.424(1), Cr1–C2 2.370(2), Cr1–C3 2.374(2), P1–C1 1.782(2), C1–P2 1.788(2), P2–C2 1.797(2), P1–C3 1.788(2), C1–P3 1.767(2), P1–C1–P2 121.2(1), P1–C1–P3 122.2(1), P3–C1–P2 120.67(9); b) UV-vis spectrum in THF, maxima and shoulders are marked with their wavelength [nm] and extinction coefficient [L mol^{-1} cm^{-1}]. The calculated spectrum using TDDFT is shown as a grey dashed line; c) cyclic voltammogram (CV) in THF (grey purple), the CV of **PPI** is shown as a dashed line.

was isolated as deep orange crystals of the composition **5**·(MgCl$_2$)$_{0.1}$ in 34 % yield. Coordination of the Cr(CO)$_3$ moiety causes a significant upfield shift of the endocyclic P atoms ($\Delta\delta(^{31}P) = -189.3$ ppm, $\delta = 23.4$ ppm, $^2J_{PP} = 66$ Hz). The exocyclic P(*p*-tol)$_3$ moiety is shifted downfield by only 3.5 ppm ($\delta =$ 28.2 ppm). Comparable coordination shifts were observed in the phosphaindenylide complex [Cr(CO)$_3$(η^5-**III**)].[15]

The solid-state structure of **5** shows the expected η^5-coordination of the **PPI** ligand (Figure 3a). However, the chromium atom is noticeably shifted off-center from the C_3P_2 ring. The Cr–P distances only differ slightly with values of 2.4149(8) Å for Cr1–P1 and 2.424(1) Å for Cr1–P2. On the other hand, the distances between chromium and carbon atoms (Cr–C) exhibit significant variations. The triphosphorus-substituted carbon atom C1 forms a short Cr–C bond (2.168(2) Å). Notably, the Cr–C1 distance is even shorter than in [Cr(CO)$_3$(η^5-C_5H_5)]$^-$ ($\emptyset_{Cr-C}$ 2.19 Å).[40] In contrast, the Cr–C bonds involving the two central quaternary carbon atoms of the C_7P_2 core are elongated by approximately 0.2 Å (Cr1–C2 2.370(2), Cr1–C3 2.374(2) Å). These Cr–C distances are actually the longest among the phosphonium-substituted indenyl complexes [Cr(CO)$_3$(η^5-**I**)], [Cr(CO)$_3$(η^5-**III**)] and **5** (see Table 1). Altogether, these structural data suggest that the η^5 coordination of the **PPI** ligand in **5** might be best described as a [$\eta^3+\eta^2$] coordination mode with three strong Cr bonds (Cr–P1, Cr–P2, Cr–C1) and two weak Cr bonds (Cr–C2, Cr–C3).

Next, the electronic structure of **5** was probed by IR and UV-vis spectroscopy. The ATR-IR spectrum of a solid sample of **5**·(MgCl$_2$)$_{0.1}$ exhibits three strong carbonyl stretching vibrations at $\tilde{\nu} = 1921$, 1855 and 1817 cm^{-1} with an average $\emptyset(\tilde{\nu}_{CO})$ of 1864 cm^{-1}. For comparison, the values of $\emptyset$ ($\tilde{\nu}_{CO}$) for [Cr(CO)$_3$(η^5-C_9H_7)]$^-$,[39] [Cr(CO)$_3$(η^5-**I**)][12] and [Cr(CO)$_3$(η^5-**III**)],[15] are given in Table 1. It is important to note that the IR data for these three complexes were obtained in solution, so a direct comparison to **5** should be approached with caution. However, a trend can still be observed: The indenyl anion in [Cr(CO)$_3$(η^5-C_9H_7)]$^-$ acts as the strongest net donor ligand and shows the smallest $\emptyset(\tilde{\nu}_{CO})$ of 1826 cm^{-1}. As anticipated, introduction of a phosphonium substituent leads to a decrease in net donor strength as evidenced from the $\emptyset(\tilde{\nu}_{CO})$ of 1845 cm^{-1} in [Cr(CO)$_3$(η^5-**I**)]. The presence of endocyclic P atoms in the indenylide ligands once again leads to an increase of $\emptyset(\tilde{\nu}_{CO})$ by ca. 18 cm^{-1}, indicating that **III** and **PPI** are the weakest net donor ligands in the series (Table 1).

Table 1. Comparison of selected analytical and calculated data of chromium tricarbonyl complexes. a: average Cr–C distance to the two central indenyl carbon atoms, b: averaged CO stretching frequencies, c: Gibbs free energy of the process [Cr(CO)$_3$(η^5-**L**)]→Cr(CO)$_3$ + **L**, d: relative contribution of π-donor interactions to the total orbital interaction energy, e: relative contribution of π-acceptor interactions to the total orbital interaction energy.

	$\emptyset$(Cr–C) [Å][a]	$\emptyset(\tilde{\nu}_{CO})$ [cm^{-1}][b]	$\Delta G_{diss.}$ [kcal mol^{-1}][c]	$\Delta E_{rel.}^{L\rightarrow M}$ [%][d]	$\Delta E_{rel.}^{M\rightarrow L}$ [%][e]
[Cr(η^5-C_9H_7)(CO)$_3$]$^-$[39]	–	1826	65.6 (100 %)	66	19
[Cr(η^5-**I**)(CO)$_3$][12]	2.27	1845	51.6 (79 %)	61	23
[Cr(η^5-**III**)(CO)$_3$][15]	2.32	1862	53.3 (81 %)	51	33
[Cr(η^5-**PPI**)(CO)$_3$] (**5**)	2.37	1864	58.2 (89 %)	56	31

Further insights were gained from the UV-vis spectrum of compound **5**. In THF, the spectrum exhibits two broad absorption bands with maximum wavelengths at $\lambda_{max} = 311$ and 433 nm. Through TDDFT calculations, it was determined that the spectrum is primarily influenced by MLCT (metal to ligand charge transfer) processes (see the SI, section 4.4). The presence of these transitions indicates that the **PPI** ligand indeed acts as a π-accepting ligand. Thus, the UV-vis data suggest that the lower net donor strength of **PPI**, in comparison to $[Cr(CO)_3(\eta^5\text{-}C_9H_7)]^-$, could be attributed to the considerable π-acceptor capability of **PPI** rather than solely the reduction in π-donor strength.

To obtain a more conclusive understanding of the ligand properties of **PPI**, we focused on examining the strength of the interactions between $[C_9H_7]^-$, **I**, **III**, and **PPI** with a $Cr(CO)_3$ fragment by calculating the Gibbs free energy, $\Delta G_{diss.}$, of the process $[Cr(CO)_3(\eta^5\text{-}\mathbf{L})] \rightarrow Cr(CO)_3 + \mathbf{L}$. Additionally, we performed EDA-NOCV calculations (energy decomposition analysis based on natural orbitals of chemical valence).[41] This analysis enables the breakdown of the overall orbital interaction energy, $\Delta E^{orb.}$, between two fragments into specific orbital pairs. Consequently, it allows to quantify the relative contributions of π-donor and π-acceptor interactions ($\Delta E^{L\rightarrow M}$ and $\Delta E^{M\rightarrow L}$, respectively). The summarized results for the complexes $[Cr(CO)_3(\eta^5\text{-}C_9H_7)]^-$, $[Cr(CO)_3(\eta^5\text{-}\mathbf{I})]$, $[Cr(CO)_3(\eta^5\text{-}\mathbf{III})]$ and **5** are listed in Table 1 (see the SI, section 4.5 for details).

As anticipated, the indenyl anion $[C_9H_7]^-$, shows the highest $\Delta G_{diss.}$ and is the strongest π-donor and weakest π-acceptor with $\Delta E^{L\rightarrow M}$ accounting for 66% and $\Delta E^{M\rightarrow L}$ accounting for 19% of ΔE^{orb}. For the phosphonium-substituted indenylide ligand **I**, slightly lower contributions of π-donor interactions and somewhat increased π-acceptor strength were found (61% and 23%, respectively). In line with expectation, the bonds between the ligand and the $Cr(CO)_3$ fragment are weakened compared to $[Cr(CO)_3(\eta^5\text{-}C_9H_7)]^-$ ($\Delta G_{diss.} = 51.6$ kcal mol^{-1} vs. 65.6 kcal mol^{-1}). For the phosphaindenylide **III**, a significant increase of the π-acceptor strength and simultaneous decrease of π-donor interactions is found compared to $[Cr(CO)_3(\eta^5\text{-}C_9H_7)]^-$ (33% and 51% respectively). However, despite this drop in π-donor interactions, the chromium tricarbonyl fragment in $[Cr(CO)_3(\eta^5\text{-}\mathbf{III})]$ is bound marginally stronger as in $[Cr(CO)_3(\eta^5\text{-}\mathbf{I})]$, indicated by the slightly higher value of $\Delta G_{diss.} = 53.3$ kcal mol^{-1}. This finding is in line with our hypothesis that introduction of P atoms to the indenyl core would increase the metal-ligand bond strength by increased π-acceptor interactions. Introduction of a second P atom to the indenyl core has an even more pronounced effect. In **5**, $\Delta G_{diss.}$ is the highest among the considered zwitterionic indenylide complexes and amounts to 89% of the value found for $[Cr(CO)_3(\eta^5\text{-}C_9H_7)]^-$ (58.2 kcal mol^{-1}) indicating a rather strong interaction between the $Cr(CO)_3$ fragment and **PPI**. Surprisingly, despite the presence of two P atoms within the indenyl core, **PPI** exhibits a slightly weaker π-acceptor strength $\Delta E^{M\rightarrow L}$, but stronger π-donor capability, $\Delta E^{L\rightarrow M}$ compared to the monophosphaindenylide ligand **III** (31% and 56%, respectively). This somewhat counterintuitive result might be related to the biradical character of **PPI**. Strong π-donor properties were also observed for a phosphorus-containing four-membered biradicaloid, the bis(imidazolium)-substituted diphosphete diide $IPr_2C_2P_2$ (**IDP**).[19]

During our DFT investigations on complex **5**, we noticed that the HOMO was essentially a filled 3d orbital on Cr, while the LUMO was mainly located at the **PPI** ligand (see the SI, section 4.6). Furthermore, a cyclic voltammetry experiment revealed the redox activity of **PPI**. Two redox events were observed, an oxidation at $E = -0.30$ V and a reduction at $E = -2.95$ V vs. Fc/Fc^+ (peak potentials at a scan rate of 100 mV s^{-1}, $[n\text{Bu}_4\text{N}]PF_6$ as electrolyte, THF). Together with the presence of MLCT processes in the UV-vis spectrum of **5**, we thus wondered whether ligand-centered redox processes might occur in **5**. To obtain some initial insights, we conducted cyclic voltammetry measurements using the same experimental conditions as before. The CV of **5** and **PPI** are shown in Figure 3c (see the SI, section 3 for details). Three redox processes are observed, a quasi-reversible oxidation at $E_{1/2} = -0.06$ V, and two irreversible reductions at peak potentials of $E = -2.45$ V and -3.09 V (all values vs. Fc/Fc^+). Tentatively, the oxidation event is assigned to the one electron-oxidation $\mathbf{5} - e^- \rightarrow [\mathbf{5}]^{\bullet+}$. Judging from the spin-density of the radical cation $[\mathbf{5}]^{\bullet+}$, this oxidation predominantly takes place at the chromium center (see the SI, section 4.6). This hypothesis is further supported by the previously described one-electron oxidation of the phosphonium-substituted cyclopentadienylide complex $[Cr(CO)_3(\eta^5\text{-}C_5H_4PPh_2Me)]$ which yields the chromium-centered radical species $[Cr(CO)_3(\eta^5\text{-}C_5H_4PPh_2Me)]^{\bullet+}$.[42] In contrast, based on the analysis of the spin-density calculation for the radical anion $[\mathbf{5}]^{\bullet-}$, it appears that the initial reduction event $\mathbf{5} + e^- \rightarrow [\mathbf{5}]^{\bullet-}$ predominantly occurs at the ligand, implying that **PPI** may indeed serve as a redox non-innocent ligand (see the SI, section 4.6).

Conclusions

Our study presents the isolation of **PPI**, a novel member of zwitterionic indenylides. A detailed theoretical and experimental investigation of its electronic structure reveals a considerable biradical character. Through an in-depth analysis of a chromium tricarbonyl complex, **5**, it became evident that the introduction of two phosphorus atoms into the indenyl framework strongly alters the ligand properties of **PPI** compared to the parent phosphonium-substituted indenyl anion. As anticipated, this modification renders **PPI** a simultaneous π-donor and π-acceptor, making it a zwitterionic ligand that still exhibits strong binding to the chromium tricarbonyl fragment. This modification potentially overcomes the drawback of zwitterionic cyclopentadienylides and indenylides, which generally tend to form weaker metal-ligand bonds.[6]

Notably, the strong bonding between **PPI** and the chromium fragment is primarily attributed to the interaction with the PCP-fragment of the C_7P_2 core, while the bonds to the two central carbon atoms of the indenyl core are comparatively weak. This observation suggests a potentially significant contribution of the indenyl effect on the reactivity of complex **5**, as well as other metal complexes incorporating the **PPI** ligand.

Additionally, our cyclic voltammetry experiments indicate the possibility of ligand-centered redox processes in **5**. This finding again highlights the potential of **PPI** as a promising ligand for the development of novel reactivity patterns in the activation of electron-rich substrates. Further exploration of **PPI** and its metal complexes are currently underway in our laboratories.

Experimental Section

General Methods. All reactions and manipulations were carried out under an argon atmosphere using standard Schlenk and glovebox techniques unless stated otherwise. Solvents were either obtained from an MBraun Solvent Purification System, or dried and stored according to common procedures.[43] $H_2C{=}P(p\text{-tol})_3$ was synthesised according to a literature procedure.[44] Magnesium was activated by heating under vacuum followed by vigorous stirring for 3d under an argon atmosphere. All other compounds are commercially available. NMR spectra were recorded with Bruker spectrometers at room temperature unless stated otherwise. UV-Vis spectra were recorded on an Agilent Cary 5000 Uv-Vis-NIR machine. ATR spectra were collected on a Bruker-alpha FT-IR-spectrometer. No unexpected or unusually high safety hazards were encountered.

Synthetic procedures

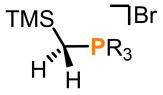

In a 500 mL round bottomed Schlenk flask, a solution of bromotrimethylsilane (50 ml, 58.5 g, 381 mmol, 6.7 eq.) in 100 mL toluene was stirred vigorously at room temperature. A solution of $(p\text{-tol})_3P{=}CH_2$ (18 g, 56.4 mmol, 1.0 eq) in 250 mL of a hexane/toluene mixture (1:1 v/v) was added slowly over the course of 20 minutes. After the addition was finished, the resulting suspension was filtered through a G3 sintered glass frit. Drying of the solid residue *in vacuo* yields 25.00 g of a mixture of $[(p\text{-tol})_3PC(TMS)H_2]Br$ and $[(p\text{-tol})_3PCH_3]Br$ (8:1). The crude product was used without further purification. The NMR spectroscopic data agree with those previously reported for $[(p\text{-tol})_3PC(TMS)H_2]I$.[45] **^{1}H NMR** ($CD_2Cl_2$, 300.1 MHz): $\delta = -0.00$ (s, 9 H, $Si(CH_3)_3$), 2.47 (s, 9 H, *para*-CH_3), 2.97 (d, $^2J(^1H, ^{31}P) = 18.5$ Hz, 1 H, $PCH_2(TMS)$), 7.47 (m, 6 H, *meta-H*), 7.70 (m, 6 H, *ortho-H*) ppm. **^{13}C{^{1}H} NMR** (CD_2Cl_2, 100.6 MHz): $\delta = 0.2$ (d, $^3J(^{13}C, ^{31}P) = 3$ Hz, 3 C, $Si(CH_3)_3$), 10.2 (d, $^1J(^{13}C, ^{31}P) = 45.8$ Hz, 1 C, PCH_2TMS), 21.6 (d, $^5J(^{13}C, ^{31}P) = 2$ Hz, 3 C, *para*-CH_3), 130.9 (d, $^2J(^{13}C, ^{31}P) = 13$ Hz, 3 C, *meta*-C^{ar}), 118.1 (d, $^1J(^{13}C, ^{31}P) = 90$ Hz, 3 C, PC^{ar}), 133.3 (d, $^2J(^{13}C, ^{31}P) = 11$ Hz, 3 C, *ortho*-C^{ar}), 146.1 (d, $^4J(^{13}C, ^{31}P) = 3$ Hz, 3 C, *para*-C^{ar}) ppm. **^{31}P{^{1}H} NMR** (CD_2Cl_2, 121.5 MHz): $\delta = 23.0$ (s, 1P, Ar_3P) ppm.

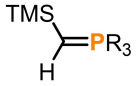

A 500 mL round bottomed Schlenk flask was equipped with a stirrer bar and charged with a mixture of $[(p\text{-tol})_3PC(TMS)H_2]Br$ and $[(p\text{-tol})_3PCH_3]Br$ (24.83 g, obtained as described above) and sodium bis(trimethylsilyl)amide (9.66 g, 52.69 mmol, 1.0 eq.) Upon addition of 250 mL toluene a lemon-yellow suspension was obtained. The mixture was stirred at room temperature for 16 h. Filtration through a G4 sintered glass frit gives a yellow, clear solution. The residual solid was extracted with 2×20 mL hexane. The solvent was removed from the combined filtrates and thorough drying *in vacuo* gives a 8:1 mixture of $(p\text{-tol})_3PC(TMS)H$ and $(p\text{-tol})_3PCH_2$ as a yellow solid (20.59 g), which can directly be used for the synthesis of $(p\text{-tol})_3PC(TMS)_2$ (**2**). Pure samples of $(p\text{-tol})_3PC(TMS)H$ were obtained by recrystallization from hot hexane. **^{1}H NMR** (C_6D_6, 300.1 MHz): $\delta =$ 0.31 (s, 9 H, $Si(CH_3)_3$), 0.39 (d, $^2J(^1H, ^{31}P) = 9.1$ Hz, 1 H, P*CH*TMS), 2.00 (s, 9 H, *para*-CH_3), 6.92 (m, 6 H, *meta-H*), 7.73 (m, 6 H, *ortho-H*) ppm. **^{13}C{^{1}H} NMR** (C_6D_6, 100.6 MHz): $\delta = -0.8$ (d, $^1J(^{13}C, ^{31}P) = 96$ Hz, 1 C, PCHTMS), 4.9 (d, $^3J(^{13}C, ^{31}P) = 4$ Hz, 3 C, $Si(CH_3)_3$), 21.2 (d, $^5J(^{13}C, ^{31}P) =$ 2 Hz, 3 C, *para*-CH_3), 129.4 (d, $^2J(^{13}C, ^{31}P) = 12$ Hz, 3 C, *meta*-C^{ar}), 132.6 (d, $^1J(^{13}C, ^{31}P) = 86$ Hz, 3 C, PC^{ar}), 133.5 (d, $^2J(^{13}C, ^{31}P) = 10$ Hz, 3 C, *ortho*-C^{ar}), 141.2 (d, $^4J(^{13}C, ^{31}P) = 3$ Hz, 3 C, *para*-C^{ar}) ppm. **^{31}P{^{1}H} NMR** (C_6D_6, 121.5 MHz): $\delta = 18.6$ (s, 1P, Ar_3P) ppm.

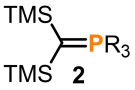

2

In a 500 mL round bottomed Schlenk flask, a solution of a 8:1 mixture of $(p\text{-tol})_3PC(TMS)H$ and $(p\text{-tol})_3PCH_2$ (10.93 g) in 250 mL toluene was stirred vigorously at room temperature. Bromotrimethylsilane (3.1 ml, 3.6 g, 28.0 mmol, 1.0 eq.) was added dropwise via syringe. The resulting mixture was stirred for 16 h. Afterwards, the mixture was filtered, and the solid residue was suspended in hexane (200 mL). Addition of sodium bis(trimethylsilyl)amide (5.13 g, 28.0 mmol, 1.0 eq.) yielded a yellow suspension. After stirring for 16 h, the mixture was filtered, and the residue was washed with hexane (2×20 mL). Then, the combined hexane fractions were reduced to 100 mL. Storing the hexane solution at −18 °C yielded yellow crystals of $(p\text{-tol})_3P{=}CTMS_2$ (7.70 g, 60 %). **^{1}H NMR** (THF-d_8, 400.1 MHz): $\delta = -0.16$ (s, 18 H, $Si(CH_3)_3$), 2.41z (s, 9 H, *para*-CH_3), 7.26−7.29 (m, 6 H, *meta-H*), 7.64 (dd, $^3J_{PP} = 12$ Hz, $^3J_{HH} =$ 8.1 Hz, 6 H, *ortho-H*) ppm. **^{13}C{^{1}H} NMR** (C_6D_6, 100.6 MHz): $\delta = -0.8$ (d, $^1J(^{13}C, ^{31}P) = 69$ Hz, 1 C, $PCTMS_2$), 4.9 (d, $^3J(^{13}C, ^{31}P) = 4$ Hz, 3 C, $Si(CH_3)_3$), 20.4 (d, $^5J(^{13}C, ^{31}P) = 1$ Hz, 3 C, *para*-CH_3), 128.4 (d, $^2J(^{13}C, ^{31}P) = 12$ Hz, 3 C, *meta*-C^{ar}), 131.6 (d, $^1J(^{13}C, ^{31}P) = 86$ Hz, 3 C, PC^{ar}), 133.9 (d, $^2J(^{13}C, ^{31}P) = 10$ Hz, 3 C, *ortho*-C^{ar}), 140.9 (d, $^4J(^{13}C, ^{31}P) =$ 3 Hz, 3 C, *para*-C^{ar}) ppm. **^{31}P{^{1}H} NMR** (THF-d_8, 162.0 MHz): $\delta = 20.1$ (s, 1P, Ar_3P) ppm.

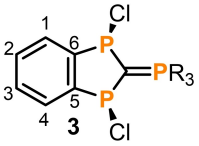

3

A solution of $C_6H_4(PCl_2)_2$ (**1**, 250 mg, 0.89 mmol, 1.00 eq.) in 1,2-difluorobenzene (DFB, 3 mL) was added to a solution of **2** (413 mg, 0.89 mmol, 1.00 eq.) in DFB (5 mL). After 16 h of stirring, the solvent was removed, and the residue was recrystallised by layering a concentrated THF solution with hexane (2.5 mL/2.5 mL) to afford **3** as a yellow solid (426 mg, 91 % yield). Some of the crystals were of sufficient quality for X-ray diffraction measurements. **^{1}H NMR** (THF-d_8, 400.1 MHz): $\delta = 2.47$ (s, 9H, $-CH_3$), 7.42 (dd, $^3J_{HH} = 8.4$ Hz, $^4J_{PP} =$ 2.7 Hz, 6H, *meta*-CH), 7.44−7.45 (m, 2H, 2,3), 7.70 (dd, $^3J_{HH} = 8.2$ Hz, $^3J_{PP} = 12.4$ Hz, 6H, *ortho*-CH), 7.79 (dq, $J = 5.9$, *3.0* Hz, 2H, 1,4) ppm. **^{13}C{^{1}H} NMR** (THF-d_8, 100.6 MHz): $\delta = 20.6$ (s, $-CH_3$), 48.9−51.2 (m, CP_3), 123.0 (dt, $^1J_{CP} = 93$ Hz, $^3J_{CP} = 3$ Hz *ipso* CP in PR_3), 128.8 (td, $J_{CP} =$ 5 Hz, 1 Hz, 2, 3), 129.4 (t, $J_{CP} = 18$ Hz, 1,4), 129.4 (d, $^2J_{CP} = 13$ Hz, *meta*-C), 134.3 (d, $^2J_{CP} = 11$ Hz, *ortho*-C), 143.5 (d, $^4J_{CP} = 3$ Hz, *para*-C), 152.6−152.9 (m, 5, 6), ppm. **^{31}P{^{1}H} NMR** (THF-d_8, 162.0 MHz): $\delta =$ 26.2 (t, $^2J_{PP} = 120$ Hz, PR_3), 133.9 (d, $^2J_{PP} = 119.8$ Hz, C_3P_2) ppm.

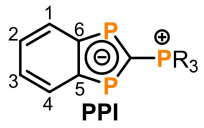

PPI

Magnesium (19 mg, 0.74 mmol, 1.10 eq.) was added to a solution of **3** (372 mg, 0.57 mmol, 1.00 eq.) in THF (5 mL). After 1 h of stirring, the mixture turned dark orange. After stirring for 20 h, volatiles were removed in vacuo and the residue was extracted with toluene (4×10 mL) and filtered through celite. Volatiles were again removed, and the residue was recrystallised by layering a THF solution with hexane (1:1 v/v) to yield **PPI**·$(MgCl_2)_{0.3}$ as a yellow solid (130 mg, 39% yield). Some of the crystals were of sufficient quality for single-crystal X-ray diffraction measurements. $\mathbf{C_{28}H_{25}P_3 \cdot (MgCl_2)_{0.3}}$, calculated (%): C 69.63, H 5.22; found (%): C 69.71, H 5.57. **^{1}H NMR** (THF-d_8, 400.1 MHz): δ = 2.47 (s, 9H, $-CH_3$), 6.96 (ddt, $^3J_{HH}$ = 6.5 Hz, J = 3.3, 1.7 Hz, 2H, 2,3), 7.40 (dd, $^3J_{HH}$ = 8.0 Hz, $^3J_{PP}$ = 2.7 Hz, 6H, *meta*-CH), 7.69–7.74 (m, 6H, *ortho*-CH), 8.28 (ddd, $^3J_{HH}$ = 6.0 Hz, J = 4.4, 2.8 Hz, 2H, 1, 4), ppm. **^{13}C{^{1}H} NMR** (THF-d_8, 100.6 MHz): δ = 20.6 (s, $-CH_3$), 119.0–119.5 (m, 2, 3), 123.2 (dt, $^1J_{CP}$ = 92 Hz, *ipso*-CP in PR_3), 128.9–129.5 (m, 1, 4), 129.3 (d, $^2J_{CP}$ = 13 Hz, *meta*-C), 134.2 (dt, $^2J_{CP}$ = 10 Hz, $^4J_{CP}$ = 3 Hz *ortho*-C), 138.0 (q, $^1J_{CP}$ = 71 Hz, CP_3), 143.7 (d, $^4J_{CP}$ = 3 Hz, *para*-C), 164.8–165.5 (m, 5, 6), ppm. **^{31}P{^{1}H} NMR** (THF-d_8, 162.0 MHz): δ = 24.7 (t, $^2J_{PP}$ = 88 Hz, PR_3), 212.7 (d, $^2J_{PP}$ = 88 Hz, C_3P_2) ppm.

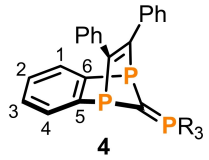

4

A mixture of **PPI**·$(MgCl_2)_{0.3}$ (40 mg, 0.08 mmol, 1.00 eq) and diphenyl acetylene (16 mg, 0.09 mmol, 1.07 eq.) was dissolved in THF and stirred at 55 °C for 60 h. Afterwards, volatiles were removed in vacuo and the resulting oil was washed with hexane (5×2 mL) to obtain **4**·$(MgCl_2)_{0.3}$ as a yellow solid (28 mg, 48%). $\mathbf{C_{42}H_{35}P_3 \cdot (MgCl_2)_{0.3}}$, calculated (%): C 76.29, H 5.34; found (%): C 76.24, H 5.59. **LIDFI-MS**: $[C_{42}H_{36}P_3]^+$ ($[M+H]^+$), m/z, calculated: 633.2036 (100%), 634.2072 (45.7%), 635.2082 (10.2%), 636.2168 (1.1%), found: 633.2007 (100%), 634.2031 (45.5%), 635.2133 (9.7%), 636.2113 (1.4%). **^{1}H NMR** (THF-d_8, 400.1 MHz): δ = 2.40 (s, 9H, $-CH_3$), 6.93–6.95 (2H, 2, 3), 6.97–7.10 (m, 10 H, C_2Ph_2), 7.27 (dd, $^3J_{HH}$ = 8.2 Hz, $^4J_{PP}$ = 2.6 Hz, 6H, *meta*-CH), 7.49–7.54 (m, 6H, *ortho*-CH), 7.82 (dq, J = 5.0, *2.6* Hz, 2H, 1,4) ppm. **^{13}C{^{1}H} NMR** (THF-d_8, 125.8 MHz): δ = 20.4 (s, $-CH_3$), 47.5 (dt, $^1J_{CP}$ = 110, 25 Hz, P_3C), 124.5–124.8 (m, 2, 3), 127.3–127.5 (m, CH-C_2Ph_2), 127.8 (d, $^1J_{CP}$ = 92 Hz, *ipso*-PR_3), 128.6–129.0 (m, 1, 4), 128.9 (d, $^3J_{CP}$ = 12 Hz, *meta*-PR_3), 133.1 (dt, $^2J_{CP}$ = 10 Hz, $^4J_{CP}$ = 2 Hz *ortho*-PR_3), 140.4–140.1 (m, *ipso*-C_2Ph_2), 141.7 (d, $^4J_{CP}$ = 3 Hz, *para*-PR_3), 161.1–161.4 (m, 5, 6), 166.7–167.0 (m, C_2Ph_2) ppm. **^{31}P{^{1}H} NMR** (THF-d_8, 162.0 MHz): δ = 14.1 (t, $^2J_{PP}$ = 102 Hz, PR_3), 63.9 (d, $^2J_{PP}$ = 102 Hz, C_3P_2) ppm.

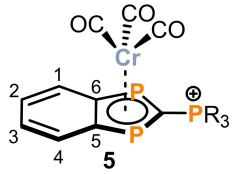

5

$[Cr(CO)_3(MeCN)_3]$ (23 mg, 0.09 mmol, 1.06 eq) was added to a solution of **PPI**·$(MgCl_2)_{0.3}$ (40 mg, 0.08 mmol, 1.00 eq) in THF. After stirring for 4 h, the mixture was filtered and layered with hexane (1:1 v/v). After 2d, **5**·$(MgCl_2)_{0.1}$ was formed as orange crystals. suitable for X-Ray diffraction measurements (17 mg, 34% yield). $\mathbf{C_{31}H_{25}Cr_1O_3P_3 \cdot (MgCl_2)_{0.1}}$, calculated (%): C 62.06, H 4.20; found (%): C 61.92, H 4.62. **^{1}H NMR** (THF-d_8, 500.1 MHz): δ = 2.48 (s, 9H, $-CH_3$), 6.91–6.93 (m, 2 H, 2,3), 7.44 (dd, $^3J_{HH}$ = 8.0 Hz, $^4J_{PP}$ = 2.7 Hz, 6H, *meta*-CH), 7.56 (dd, $^3J_{HH}$ = 8.1 Hz, $^3J_{PP}$ = 12.5 Hz, 6H, *ortho*-CH), 7.56–7.60 (m, 2H, 1, 4) ppm. **^{13}C{^{1}H} NMR** (THF-d_8, 125.8 MHz): δ = 20.6 (s, $-CH_3$), 120.9 (d, $^1J_{CP}$ = 92z Hz, *ipso* CP in PR_3), 124.3 (t, J_{CP} = 5 Hz, 2, 3), 126.3 (dd, $^1J_{CP}$ = 59 Hz, $^2J_{CP}$ = 14 Hz., 5, 6), 129.7 (d, $^2J_{CP}$ = 13 Hz, *meta*-C), 130.2–130.6 (m, 1, 4), 133.8 (dt, $^2J_{CP}$ = 11 Hz, $^4J_{CP}$ = 3 Hz *ortho*-C), 144.9 (d, $^4J_{CP}$ = 3 Hz, *para*-C), ppm (note, that the triphosphorus-substituted carbon atom could not be found due to the limited solubility of **5**·$(MgCl_2)_{0.1}$). **^{31}P{^{1}H} NMR** (THF-d_8, 202.5 MHz): δ = 23.4 (d, $^2J_{PP}$ = 66 Hz, C_3P_2), 28.2 (t, $^2J_{PP}$ = 66 Hz, PR_3) ppm.

Supporting Information

Additional references cited in the supporting information.[46–52]

Acknowledgements

Financial support (Liebig scholarship of the VCI for P.C. and ETH grant ETH-4520-1 for C.S.) is gratefully acknowledged. We thank Patrick Mollig (TU Munich) for measurement of mass spectra. P. C. expresses his immense gratitude to Evamarie Hey-Hawkins and Hansjörg Grützmacher for their invaluable guidance and support, which played a crucial role in launching his independent research career. Open Access funding enabled and organized by Projekt DEAL.

Conflict of Interests

The authors declare no conflict of interest.

Data Availability Statement

The data that support the findings of this study are available in the supplementary material of this article or from the author upon reasonable request.

Keywords: Chromium · Coordination Chemistry · Phosphorus Heterocycles · Quantum Chemistry · Ylides

[1] A. J. Hart-Davis, R. J. Mawby, *J. Chem. Soc. Inorg. Phys. Theor.* **1969**, 2403–2407.
[2] J. M. O'Connor, C. P. Casey, *Chem. Rev.* **1987**, *87*, 307–318.
[3] B. M. Trost, M. C. Ryan, *Angew. Chem. Int. Ed.* **2017**, *56*, 2862–2879.
[4] L. Atkin, D. L. Priebbenow, *Angew. Chem. Int. Ed.* **2023**, *62*, e202302175.
[5] J. H. Brownie, M. C. Baird, *Coord. Chem. Rev.* **2008**, *252*, 1734–1754.
[6] D. Kunz, F. Mazzotta, in *Advances in Organometallic Chemistry* (Eds.: P. J. Pérez, F. G. A. Stone, R. West), Academic Press, **2018**, pp. 181–231.
[7] F. Mazzotta, G. Zitzer, B. Speiser, D. Kunz, *Chem. Eur. J.* **2020**, *26*, 16291–16305.
[8] F. Mazzotta, K. W. Törnroos, D. Kunz, *Organometallics* **2020**, *39*, 3590–3601.
[9] E. J. T. Phipps, T. Rovis, *J. Am. Chem. Soc.* **2019**, *141*, 6807–6811.

[10] H. Gao, L. Hu, Y. Hu, X. Lv, Y.-B. Wu, G. Lu, *Org. Chem. Front.* **2022**, *9*, 979–988.
[11] E. Tomita, M. Kojima, Y. Nagashima, K. Tanaka, H. Sugiyama, Y. Segawa, A. Furukawa, K. Maenaka, S. Maeda, T. Yoshino, S. Matsunaga, *Angew. Chem. Int. Ed.* **2023**, *62*, e202301259.
[12] J. H. Brownie, M. C. Baird, *J. Organomet. Chem.* **2008**, *693*, 2812–2817.
[13] K. G. Fowler, S. L. Littlefield, M. C. Baird, P. H. M. Budzelaar, *Organometallics* **2011**, *30*, 6098–6107.
[14] K. Purdavaie, M. C. Baird, P. H. M. Budzelaar, *New J. Chem.* **2015**, *39*, 9429–9441.
[15] D. Gudat, S. Häp, L. Szarvas, M. Nieger, *Chem. Commun.* **2000**, 1637–1638.
[16] D. Gudat, S. Häp, M. Nieger, *J. Organomet. Chem.* **2002**, *643–644*, 181–188.
[17] I. Bakk, D. Gudat, S. Häp, M. Nieger, L. Nyulaszi, L. Szarvas, *Z. Anorg. Allg. Chem.* **2005**, *631*, 47–54.
[18] Z. Li, X. Chen, L. L. Liu, M. T. Scharnhölz, H. Grützmacher, *Angew. Chem. Int. Ed.* **2020**, *59*, 4288–4293.
[19] M. T. Scharnhölz, P. Coburger, L. Gravogl, D. Klose, J. J. Gamboa-Carballo, G. Le Corre, J. Bösken, C. Schweinzer, D. Thöny, Z. Li, K. Meyer, H. Grützmacher, *Angew. Chem. Int. Ed.* **2022**, *61*, e202205371.
[20] P. Coburger, F. Masero, J. Bösken, V. Mougel, H. Grützmacher, *Angew. Chem. Int. Ed.* **2022**, *61*, e202211749.
[21] M. Scharnhölz, *Biradicaloids as Ligands in Iron Carbonyl Complexes*, ETH Zürich, **2023**.
[22] O. Kühl, *Phosphorus-31 NMR Spectroscopy: A Concise Introduction for the Synthetic Organic and Organometallic Chemist*, Springer Science & Business Media, **2008**.
[23] Deposition Numbers 2307615 (**3**), 2292489 (**PPI**) and 2292488 (**5**) contain the supplementary crystallographic data for this paper. These data are provided free of charge by the joint Cambridge Crystallographic Data Centre and Fachinformationszentrum Karlsruhe Access Structures service.
[24] F. H. Allen, O. Kennard, D. G. Watson, L. Brammer, A. G. Orpen, R. Taylor, *J. Chem. Soc. Perkin Trans. 2* **1987**, S1–S19.
[25] JosephJ. Mullins, *J. Chem. Educ.* **2012**, *89*, 834–836.
[26] F. Neese, F. Wennmohs, U. Becker, C. Riplinger, *J. Chem. Phys.* **2020**, *152*, 224108.
[27] E. Matito, M. Duran, M. Solà, *J. Chem. Phys.* **2005**, *122*, 014109.
[28] Z. Chen, C. S. Wannere, C. Corminboeuf, R. Puchta, P. v. R. Schleyer, *Chem. Rev.* **2005**, *105*, 3842–3888.
[29] B. Braïda, A. Lo, P. C. Hiberty, *ChemPhysChem* **2012**, *13*, 811–819.
[30] F. E. Penotti, D. L. Cooper, P. B. Karadakov, *Int. J. Quantum Chem.* **2019**, *119*, e25845.
[31] H. M. Tuononen, R. Suontamo, J. Valkonen, R. S. Laitinen, *J. Phys. Chem. A* **2004**, *108*, 5670–5677.
[32] P. Coburger, R. Wolf, H. Grützmacher, *Eur. J. Inorg. Chem.* **2020**, *2020*, 3580–3586.
[33] E. Miliordos, K. Ruedenberg, S. S. Xantheas, *Angew. Chem. Int. Ed.* **2013**, *52*, 5736–5739.
[34] J. Bresien, D. Michalik, A. Schulz, A. Villinger, E. Zander, *Angew. Chem. Int. Ed.* **2021**, *60*, 1507–1512.
[35] T. Beweries, R. Kuzora, U. Rosenthal, A. Schulz, A. Villinger, *Angew. Chem. Int. Ed.* **2011**, *50*, 8974–8978.
[36] A. Hinz, A. Schulz, W. W. Seidel, A. Villinger, *Inorg. Chem.* **2014**, *53*, 11682–11690.
[37] L. Chojetzki, A. Schulz, A. Villinger, R. Wustrack, *Z. Anorg. Allg. Chem.* **2020**, *646*, 614–624.
[38] Z. Li, Y. Hou, Y. Li, A. Hinz, X. Chen, *Chem. Eur. J.* **2018**, *24*, 4849–4855.
[39] A. Ceccon, A. Gambaro, F. Gottardi, S. Santi, A. Venzo, *J. Organomet. Chem.* **1991**, *412*, 85–94.
[40] R. Y. C. Shin, V. W. L. Ng, L. L. Koh, G. K. Tan, L. Y. Goh, R. D. Webster, *Organometallics* **2007**, *26*, 4555–4561.
[41] M. P. Mitoraj, A. Michalak, T. Ziegler, *J. Chem. Theory Comput.* **2009**, *5*, 962–975.
[42] J. H. Brownie, M. C. Baird, D. R. Laws, W. E. Geiger, *Organometallics* **2007**, *26*, 5890–5901.
[43] W. L. F. Armarego, C. L. L. Chai, *Purification of Laboratory Chemicals*, Butterworth-Heinemann, Oxford, **2009**.
[44] G. Wittig, H.-D. Weigmann, M. Schlosser, *Chem. Ber.* **1961**, *94*, 676–689.
[45] G. Singh, *Phosphorus Sulfur Silicon Relat. Elem.* **1994**, *97*, 125–139.
[46] G. M. Sheldrick, *Acta Crystallogr. Sect. A* **2008**, *64*, 112–122.
[47] F. Neese, *Wiley Interdiscip. Rev.: Comput. Mol. Sci.* **2018**, *8*, e1327.
[48] R. A. Kendall, H. A. Früchtl, *Theor. Chem. Acc.* **1997**, *97*, 158–163.
[49] F. Neese, F. Wennmohs, A. Hansen, U. Becker, *Chem. Phys.* **2009**, *356*, 98–109.
[50] S. Grimme, J. Antony, S. Ehrlich, H. Krieg, *J. Chem. Phys.* **2010**, *132*, 154104.
[51] S. Grimme, S. Ehrlich, L. Goerigk, *J. Comput. Chem.* **2011**, *32*, 1456–1465.
[52] T. Lu, F. Chen, *J. Comput. Chem.* **2012**, *33*, 580–592.

Manuscript received: September 12, 2023
Accepted manuscript online: November 30, 2023
Version of record online: January 10, 2024